

Pressure Perturbations and Upslope Flow over a Heated, Isolated Mountain

BART GEERTS, QUN MIAO, AND J. CORY DEMKO

University of Wyoming, Laramie, Wyoming

(Manuscript received 29 January 2008, in final form 14 April 2008)

ABSTRACT

Surface and upper-air data, collected as part of the Cumulus Photogrammetric, In Situ, and Doppler Observations (CuPIDO) experiment during the 2006 monsoon season around the Santa Catalina Mountains in southeast Arizona, are used to study the diurnal variation of the mountain-scale surface convergence and its thermal forcing. The thermal forcing is examined in terms of a horizontal pressure gradient force, which is derived assuming hydrostatic balance. The mountain is ~ 30 km in diameter, ~ 2 km high, and relatively isolated. The environment is characterized by weak winds, a deep convective boundary layer in the afternoon, and sufficient low-level moisture for orographic cumulus convection on most days.

The katabatic, divergent surface flow at night and anabatic, convergent flow during the day are in phase with the diurnal variation of the horizontal pressure gradient force, which points toward the mountain during the day and away from the mountain at night. The daytime pressure deficit over the mountain of 0.5–1.0 mb is hydrostatically consistent with the observed 1–2-K virtual potential temperature excess over the mountain. The interplay between surface convergence and orographic thunderstorms is examined, and the consequence of deep convection (outflow spreading) is more apparent than its possible trigger (enhanced convergence).

1. Introduction

Significant research has been conducted on flow and pressure variations around an isolated mountain in stratified flow. In such flow a mostly hydrostatic high pressure anomaly is found on the upwind side of the mountain, and a low on the downwind side (e.g., Baines 1979; Smith 1980; Hunt and Snyder 1980; Mass and Ferber 1990; Vosper 2000). Relatively little is known about pressure variations around an isolated, heated mountain in summer under weak flow, when a deep convective boundary layer (CBL) develops around and over the mountain during the daytime. Most of the work on this topic has addressed large-scale mountains or plateaus, such as the Rocky Mountains (e.g., Reiter 1982; Reiter and Tang 1984; Tucker 1999). Pressure variations over heated mountains are important because they drive horizontal convergence and upslope flow over the mountain, and this in turn sustains orographic convection and precipitation.

Our interest is in mountains large enough to sustain

mountain-scale convergence in the CBL and, under suitable stability and cumulus development, but small enough that the solenoidal flow response to elevated heating is quasi-instantaneous. It is generally accepted that under weak stratification ($N \rightarrow 0$ and $Fr \rightarrow \infty$, where N is the Brunt–Väisälä frequency and Fr is the Froude number) and weak wind, a thermally direct solenoidal or “heat island” circulation develops over a mountain as the surface net radiation increases, with anabatic flow converging over the mountain. This has been established mainly using numerical simulations with idealized terrain profiles (e.g., Thyer 1966; McNider and Pielke 1981; Bader and Mckee 1983; Banta 1986; de Wekker et al. 1998). A vertical cross section of this circulation is shown schematically in Fig. 1. Flow aloft is expected to have some impact on surface pressure and flow patterns if the CBL domes above the mountain.

Few observational studies document pressure variations and anabatic flow development around a heated mountain. One challenge remains the altitude differences of station observations. Fujita et al. (1962) used surface pressure departures from the daily mean to document lower pressure values over the mountain during the day, especially on the sun-facing side of the mountain. The onset and peak times of the pressure

Corresponding author address: Bart Geerts, Department of Atmospheric Sciences, University of Wyoming, Laramie, WY 82071.
E-mail: geerts@uwyo.edu

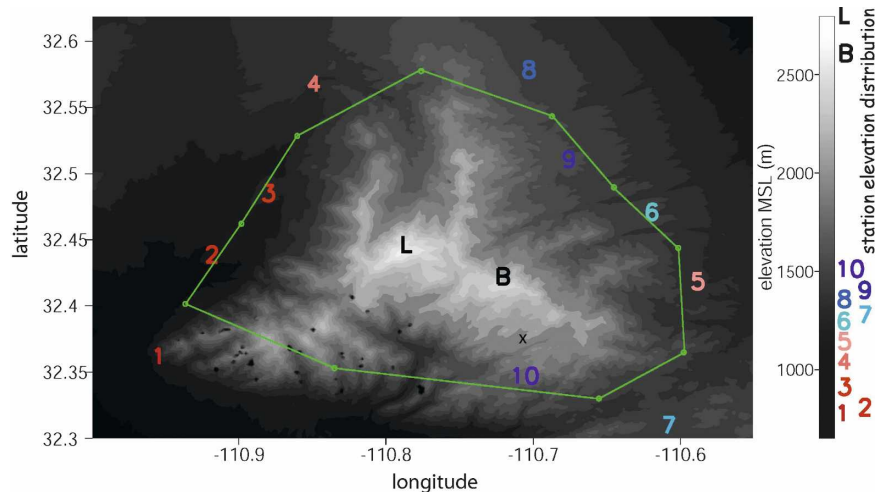


FIG. 2. Location of the surface stations around the Catalina Mountains. The ISFF stations are labeled with numbers from 1 to 10, ranked and colored by elevation: the Mt. Lemmon station (L), the Mt. Bigelow flux tower (B), and Windy Point (x). The distribution of station elevations is shown on the right of the elevation key. The green polygon connects the midpoints between the 10 ISFF stations.

humidity sensors and 3D sonic anemometers (Table 1). The vegetation around the ISFF stations was typical for the upper Sonoran Desert: broadly separated paloverde and ocotillo trees dominated, interspersed with saguaro cacti. Thus, the land surface was largely bare soil, for which significant rainfall can dramatically alter the surface energy balance. The ISFF pressure sensor was a Vaisala PTB220B, a highly stable instrument with an accuracy of 0.25 hPa at the temperature range encountered during CuPIDO. (More information about the sensors and the siting of the ISFF stations can be online found at <http://www.eol.ucar.edu/rtf/projects/CuPIDO/isff/>.)

We also use meteorological data from two mountain stations: one is a continuously operating 30-m flux tower located on Mt. Bigelow and the other is an astronomical observatory on the Santa Catalina Mountains' highest point, Mt. Lemmon. [The tower at Mt.

Bigelow is operated by the Sustainability of semi-Arid Hydrology and Riparian Areas (SAHRA) at the University of Arizona; its instruments are described online at <http://www.sahra.arizona.edu/research/TA1/towers/>.] The meteorological data acquisition system at Mt. Lemmon was struck by lightning on 19 August 2006, resulting in a lack of Mt. Lemmon data between 19 and 31 August. All data were collected at 5-min intervals or better, except for the Mt. Lemmon data, which were hourly. Therefore, in any comparison that includes all 12 stations, all data are reduced to a 60-min resolution by centered averaging.

The altitude of the 12 stations ranges from 840 m on the southwestern side to 2779 m (the Mt. Lemmon astronomical observatory), a difference of 1939 m. We also use data from the National Lightning Detection Network (NLDN) and radiosonde data, both from the National Weather Service (NWS) Tucson office (TUS) located on the University of Arizona campus, and from the Mobile Global Positioning System (GPS) Advanced Upper-Air Sounding System (MGAUS), deployed as part of CuPIDO.

Surface measurements at the 10 ISFF stations, at the Mt. Bigelow flux tower, and at the Mt. Lemmon observatory were available for an overlapping period of 58 days in the summer of 2006 (22 June–18 August). Thus, the present analysis is focused on that period. This period can be subdivided in two parts: the first period (22 June–25 July) witnessed several orographic afternoon thunderstorms but the soil remained rather dry and the surface latent heat fluxes for the four ISFF flux stations

TABLE 1. Summary of ISFF stations deployed in CuPIDO.

Site	No.	Flux?	Elev (m)	
Pusch Ridge Archery	SW	1	No	840
Catalina Water Tower	W	2	No	853
Golder Ranch	WNW	3	No	961
Rancho Solano	NNW	4	Yes	1044
Campo Bonito	N	8	No	1305
Stratton Canyon	NE	9	Yes	1365
Davis Mesa	ENE	6	Yes	1234
Lone Hill	E	5	No	1141
Bellota Ranch	SSE	7	Yes	1270
Bug Springs	S	10	No	1500

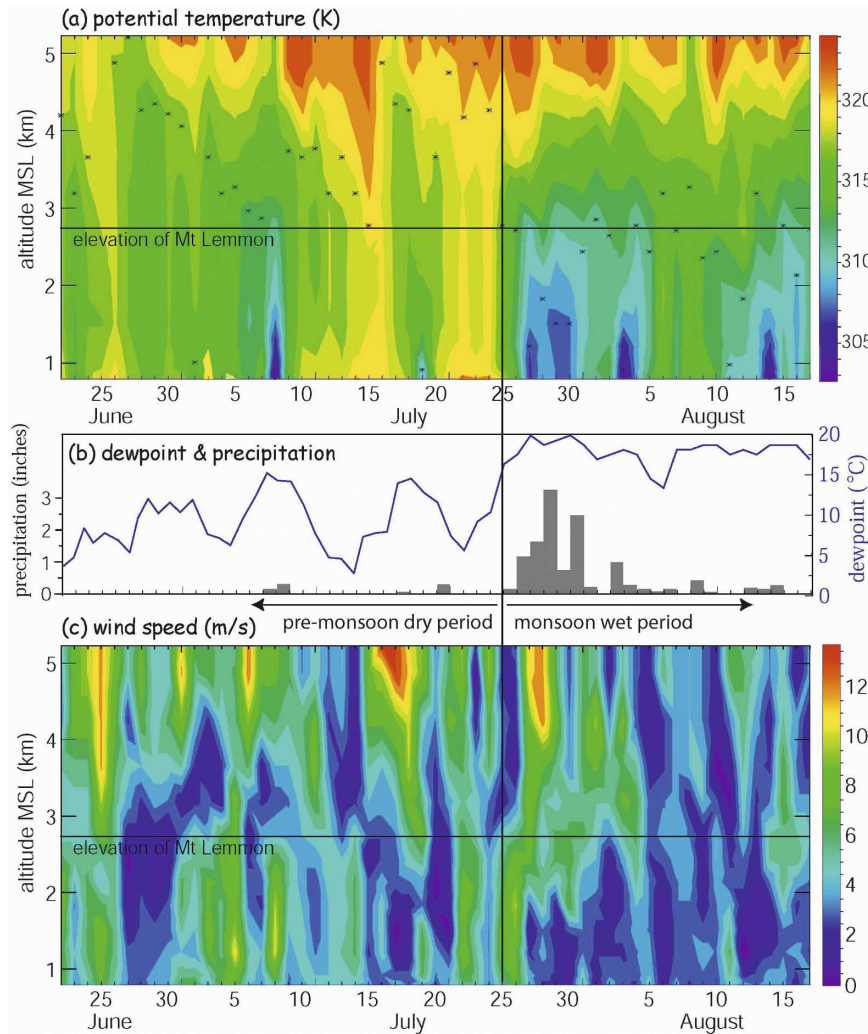


FIG. 3. Time-height plots of (a) potential temperature and (c) wind speed for the 58-day analysis period in 2006. The data are based on the 0000 UTC TUS (Tucson, AZ) radiosondes. The stars in (a) indicate the depth of the well-mixed boundary layer. The horizontal line shows the elevation of Mt. Lemmon. (b) The 24-h mean dewpoint and the average daily precipitation for the 10 ISFF stations.

remained small. We refer to it as the premonsoon dry period, even though the daily mean dewpoint exceeded the NWS's threshold for monsoon conditions in Tucson (12.2°C) on several days (Fig. 3b). The average rainfall at the 10 ISFF stations between 26 July and 5 August 2006 amounted to 274 mm (Fig. 3b), much of it from nocturnal organized convection (Damiani et al. 2008). This exceptionally heavy rainfall resulted in near-saturated soils, local flooding, and a latent heat flux that far exceeded the sensible heat flux at any time of the day. We refer to the period of 26 July–18 August as the monsoon wet period.

High temperatures and a deep CBL prevailed during the premonsoon dry period (Fig. 3a). To establish the

CBL depth, we use the operational 0000 UTC soundings, released at TUS about 3.8 h after local solar noon (LSN). The CBL depth is defined as the midpoint between two consecutive levels in a sounding where the potential temperature increases by at least 1 K, and that increase is sustained. The midpoint (rather than the base) is chosen because of the coarse vertical resolution of the soundings. Sometimes this method yields an unrealistically shallow CBL, especially on some days with thunderstorms, but Fig. 3a demonstrates that generally the CBL exceeded the height of the mountain during the premonsoon dry period, and that the CBL top above TUS was often near the mountaintop level during the wet period.

Winds were generally weak ($<5 \text{ ms}^{-1}$) below the elevation of Mt. Lemmon, especially during the wet period (Fig. 3c). On some days stronger winds ($>10 \text{ ms}^{-1}$) penetrated down to 1–2 km above Mt. Lemmon. On such days the interaction between large-scale mean flow and the mountain may have impacted the pressure, temperature, and flow distribution around the mountain. Yet on those days (except on 27–28 July) the CBL depth exceeded the mountain top height, and the observed circular asymmetry of surface flow at the ISFF stations was weak, so the interaction with the large-scale flow is ignored.

b. Pressure perturbations and the horizontal pressure gradient force

A pressure perturbation is a departure from a “mean” or “basic-state” value. The mean pressure is usually defined as the value that is hydrostatically consistent with the mean density profile. Pressure perturbations near mountains can be both hydrostatic and nonhydrostatic.

According to hydrostatic balance, a higher temperature over some depth in the atmosphere implies a lower pressure below this layer. During the summer the mature CBL is usually deeper than the altitude of Mt. Lemmon (Fig. 3a), thus, the CBL top is sketched above the mountain top in Fig. 1. To estimate the impact of a temperature anomaly within the CBL over the mountain (as shown in Fig. 1) on the air pressure below, we assume a constant virtual potential temperature (θ_v) profile. Then the anomalous pressure (p'_{ref}) at the reference level (z_{ref}) due to a θ_v anomaly (θ'_v) is linearly proportional to the θ_v anomaly and (to a good approximation) linearly proportional to its depth δ :

$$p'_{\text{ref}} = -\frac{\delta}{R_d} \frac{\theta'_v}{\theta_v^2} g p_o^K \left(p_{\text{top}}^K + \frac{p_o^K g \delta}{c_p \theta_v} \right)^{(1-K)/K}. \quad (1)$$

This relationship is derived from hydrostatic balance and the ideal gas law, assuming that θ'_v is height independent over the layer depth δ , that the perturbations are small compared to the mean values, and that the pressure on top of the CBL is uniform ($p = p_{\text{top}}$ at $z_{\text{top}} = z_{\text{ref}} + \delta$). In (1), R_d is the ideal gas constant for dry air, c_p is the specific heat under constant pressure, g is the gravitational acceleration, K is a constant ($K = (R_d/c_p) = 0.286$), and $p_o \equiv 1000 \text{ mb}$.

The average height difference between the two mountain stations and the 10 ISFF stations is 1.6 km. Thus, setting the reference level at the average altitude of the ISFF stations in the foothills and $\delta = 1.6 \text{ km}$, then a θ_v excess of 2 K over the mountain yields a pressure deficit of 1.0 mb, according to (1). Clearly this lower

pressure would occur under the mountain bedrock (Fig. 1), but the horizontal pressure gradient force is nevertheless real.

Station pressure values are normally reduced to a common height above mean sea level (MSL) in order to evaluate the horizontal pressure gradient forcing (e.g., Reiter and Tang 1984; Tucker 1999). This is not feasible in the present study because of the large variations in the altitude of the stations on and around the Santa Catalina Mountains. The hydrostatic reduction to a common height would be too sensitive to the assumed temperature profile. Rather, we define a pressure perturbation from a temporal and spatial mean, and relate the horizontal gradient of this perturbation to that of the actual pressure. This only yields a pressure gradient (not a pressure), but that is sufficient for our purpose (i.e., to infer the forcing of anabatic wind). The only assumptions are hydrostatic balance, and a relatively small horizontal scale, specified below.

First, station pressure perturbations p' are defined as departures from their 24-h station mean value, \bar{p}_t . We assume that over the scale of the mountain, at any level, the *horizontal* variation of \bar{p}_t and thus the mean geostrophic wind are insignificant; that is, $\partial \bar{p}_t / \partial r \approx 0$, where r is the radial direction from the mountain, using cylindrical coordinates. (This applies to the azimuthal direction as well, but we assume circular symmetry, for simplicity.) But clearly \bar{p}_t varies significantly with height. Next we remove \bar{p}_s , the mean of \bar{p}_t for all stations at any given time. This removes (semi) diurnal pressure variations, at least if the spatial structure of these variations is large compared to the network of stations used. Note that \bar{p}_s is a function of time only, not any spatial dimension. Thus,

$$p'' \equiv p - \bar{p}_t - \bar{p}_s. \quad (2)$$

Wind is forced by a horizontal pressure gradient, thus the question is whether we can treat the observed difference in p'' between stations ($\Delta p''$) as a measure of horizontal pressure gradient $\partial p / \partial r$. Treating the finite difference as a differential, we obtain the following from (2):

$$\begin{aligned} \Delta p'' &= \frac{\partial(p - \bar{p}_t - \bar{p}_s)}{\partial r} \Delta r + \frac{\partial(p - \bar{p}_t - \bar{p}_s)}{\partial z} \Delta z \\ &= \frac{\partial p}{\partial r} \Delta r + \frac{\partial(p - \bar{p}_t)}{\partial z} \Delta z. \end{aligned} \quad (3)$$

Assuming that both p and \bar{p}_t are in hydrostatic balance, (3) can be expressed as

$$\frac{\Delta p''}{\Delta r} = \frac{\partial p}{\partial r} - (\rho - \bar{\rho}_t) g \frac{\Delta z}{\Delta r}. \quad (4)$$

Here ρ is the air density, and $\bar{\rho}_t$ is its 24-h mean value. The term $\Delta z/\Delta r$ is the average slope S of the terrain. Using the ideal gas law, and assuming that the perturbation $\rho - \bar{\rho}_t$ is small enough that differential calculus applies, (4) becomes

$$\frac{\Delta p''}{\Delta r} = \frac{\partial p}{\partial r} - (p - \bar{p}_t)g \frac{\rho}{p} S + (T_v - \bar{T}_{v,t})g \frac{\rho}{T_v} S$$

or

$$\frac{\partial p}{\partial r} = \frac{\Delta p''}{\Delta r} + (p - \bar{p}_t)g \frac{\rho}{p} S - (T_v - \bar{T}_{v,t})g \frac{\rho}{T_v} S. \quad (5)$$

Here $T_v - \bar{T}_{v,t}$ is the virtual temperature departure from the 24-h mean, for any station. Fujita et al. (1962) argued, without giving details, that observed pressure perturbation gradients between stations ($\Delta p''/\Delta x$) can be treated as *horizontal* pressure gradients [the term on the left in (5)], in other words, that the last two terms in (5) can be ignored. These two terms depend on the magnitude of the diurnal cycles of pressure and temperature, respectively. To address whether they can be ignored, we scale (5) for the differences between a mountain station and a foothill station in the Santa Catalina Mountains, and at times that the diurnal cycle terms in (5) reach their maximum value. It will be shown in section 3 that $\Delta p''$ peaks at 1.0 mb, over a distance Δr of 15 km on average, and that the maximum pressure departures from the 24 h mean [largely due to (semi) diurnal tides] at stations around the mountain, $p - \bar{p}_t$, average at 1.4 mb. The average slope between the mountain top and the ISFF stations is $S = 0.10$. Thus, the first term on the right in (5) scales as $7 \times 10^{-3} \text{ Pa m}^{-1}$, and the second term scales as $2 \times 10^{-3} \text{ Pa m}^{-1}$. The maximum values for $(T_v - \bar{T}_{v,t})$ average at 3.8 K, thus the last term on the right in (5) scales as $13 \times 10^{-3} \text{ Pa m}^{-1}$. This scale analysis indicates that the observed spatial difference in p'' is not just due to a horizontal pressure gradient, but also due to the diurnal temperature cycle. Thus, we use (5) to estimate the diurnal variation of the (hydrostatic) *horizontal pressure gradient* $\partial p/\partial r$ between the mountain and the 10 foothill stations. Because the temperature sensor at the Mt. Lemon astronomical observatory was biased by exposure to sunshine during part of the day (see section 3), we use the Mt. Bigelow tower as the reference mountain site. To evaluate the virtual temperature and pressure departures from their 24-h mean values in (5), we use average values of the two sources for which the pressure difference is computed (i.e., Mt. Bigelow and the select ISFF station).

c. Thermally forced orographic circulation

Mahrt (1982) developed the momentum equations for katabatic flow in terrain-following coordinates. The equations can be applied to upslope flow. Thus, anabatic wind can be driven by two terms: a buoyancy term and a hydrostatic thermal wind term. The buoyancy term is due to local excess in θ_v , and vanishes when the slope disappears. The thermal wind term drives a sea breeze over flat terrain, for instance. It yields upslope flow when the CBL contains a higher θ_v over the mountain. Unfortunately, we cannot estimate the thermal wind term because we do not know the horizontal variations of the CBL depth. Because the CBL was typically weakly capped in CuPIDO, we cannot assume that its top is flat. There is some evidence from simultaneous MGAUS soundings that the CBL top domed over the mountain, as sketched in Fig. 1. This is attributed to local surface heating over the mountain.

A sufficient way to quantify the forcing of anabatic flow is to consider the horizontal vorticity equation (e.g., Miao and Geerts 2007):

$$\frac{D\eta}{Dt} = \frac{g}{\theta_v} \frac{\partial \theta_v}{\partial r}. \quad (6)$$

Here D/Dt is the total derivative, $\eta = (\partial u/\partial z) - (1/r)(\partial rw/\partial r)$ is the horizontal vorticity around the mountain, and (u, w) the velocity vector in a radial cross section. A toroidal circulation, or ring vortex around the mountain, is driven by a radial gradient in θ_v . According to Eq. (1), this gradient is proportional to the hydrostatic horizontal pressure gradient force, discussed in section 2b.

The toroidal circulation includes low-level, convergent, anabatic flow, and divergent flow at some level aloft. We cannot estimate the divergent flow aloft, but the location of the ISFF stations allows an estimation of the low-level convergent component (called the *mean anabatic wind* \bar{v}_n) as follows:

$$\bar{v}_n = \frac{1}{C} \oint \mathbf{v}_n \cdot d\mathbf{s}, \quad (7)$$

where $C = \oint ds$ is the circumference of a polygon obtained by connecting the 10 midpoints between the 10 adjacent ISFF stations (Fig. 2), ds is the incremental distance along this irregular decagon, and \mathbf{v}_n is the horizontal wind component normal to vector $d\mathbf{s}$. The reason for the use of midpoints is that it positions the stations centrally near the decagon sides, and thus the station winds yield the best available estimate for \mathbf{v}_n along corresponding decagon sides. By definition, $\mathbf{v}_n > 0$ for winds blowing into the decagon. The *mountain-scale convergence* $-\nabla \cdot \mathbf{v}$ is linearly proportional to \bar{v}_n , ac-

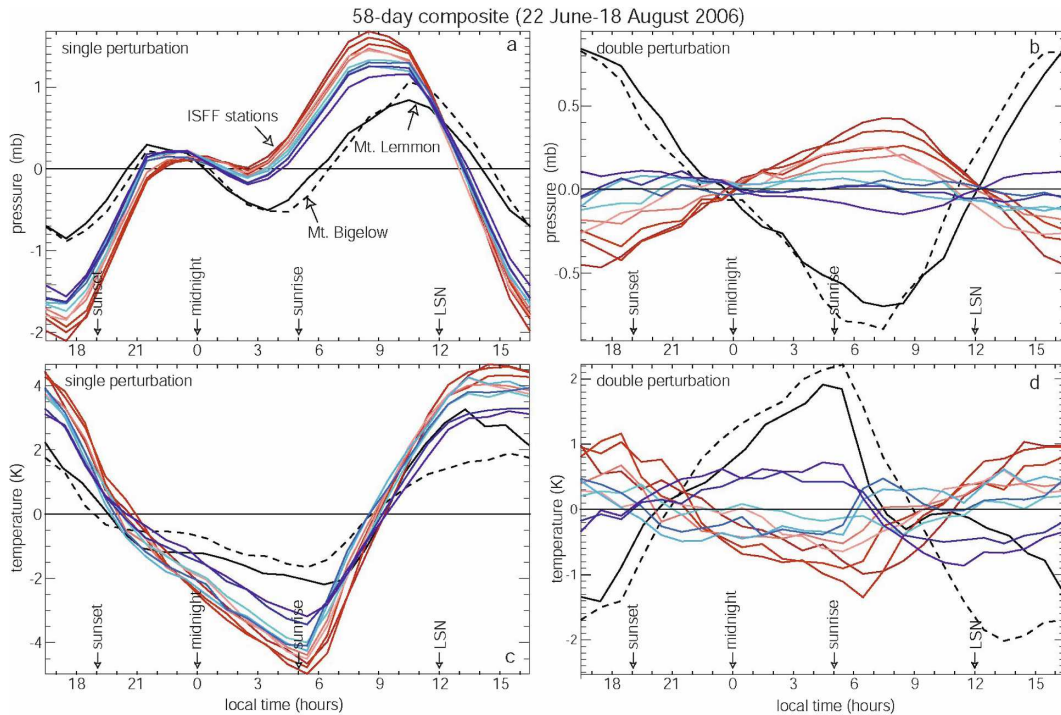


FIG. 4. Diurnal variation of pressure and temperature perturbations based on surface station data. In this and the following figures, the time is shown relative to local midnight (0729 UTC), so 12 h corresponds with local solar noon LSN (1929 UTC). The single perturbation has the 24-h mean value removed, for any station; the double perturbation also has the 12-station mean removed, at any time. The line colors match station label colors in Fig. 2. The solid black line is for Mt. Lemmon, and the dashed black line applies to Mt. Bigelow.

according to the divergence theorem (e.g., Holton 2004) and (7):

$$-\nabla \cdot \mathbf{v} = \frac{1}{A} \oint v_n ds = \frac{\bar{v}_n C}{A}. \quad (8)$$

Here A is the area contained within the decagon, $A = 576 \text{ km}^2$.

3. Diurnal trend of mountain-scale convergence and its forcing

a. Surface pressure and temperature variations around the mountain

The diurnal pattern of the “single” pressure perturbation ($p - \bar{p}_t$) is dominated by the diurnal and semi-diurnal tides, each with an amplitude of about 1.0 mb (Fig. 4a). These oscillations appear very similar for each site, but both frequencies, especially the diurnal component, have a smaller amplitude at the two mountain stations. The differences in diurnal variation of p'' ($p - \bar{p}_t - \bar{p}_s$; Fig. 4b) between stations should almost entirely be due to boundary layer processes, since the upper-atmospheric (semi) diurnal tidal variations have a

large-scale structure that is essentially uniform for our cluster of 12 stations (e.g., Hagan et al. 2002).

The difference in p'' between the mountain and the foothill stations is roughly periodic, with an amplitude of nearly 1.0 mb: the pressure is anomalously low over the mountain near midnight and peaks ~ 2 h after sunrise. It is anomalously high at the mountain sites throughout the afternoon, peaking 4–5 h after LSN. A closer examination of Fig. 4b shows that pressure perturbations are largely controlled by station altitude (color coded and shown on the right side in Fig. 2). The highest of all ISFF stations (i.e., station 10), is closest to the Mt. Lemmon curve, while the perturbation pressure trend of the low-elevation west-side stations (i.e., stations 1, 2, and 3) is most dissimilar to Mt. Lemmon’s.

The dependence of $\Delta p''$ on station elevation differences appears to be the result of differences in the diurnal virtual temperature variation integrated over the depth of the local boundary layer. We do not have temperature profile data, but within the well-mixed CBL, surface θ_s is a sufficient surrogate. Mt. Bigelow has the smallest diurnal temperature variation (Fig. 4c), mainly because the nighttime cooling is less, thus, it is

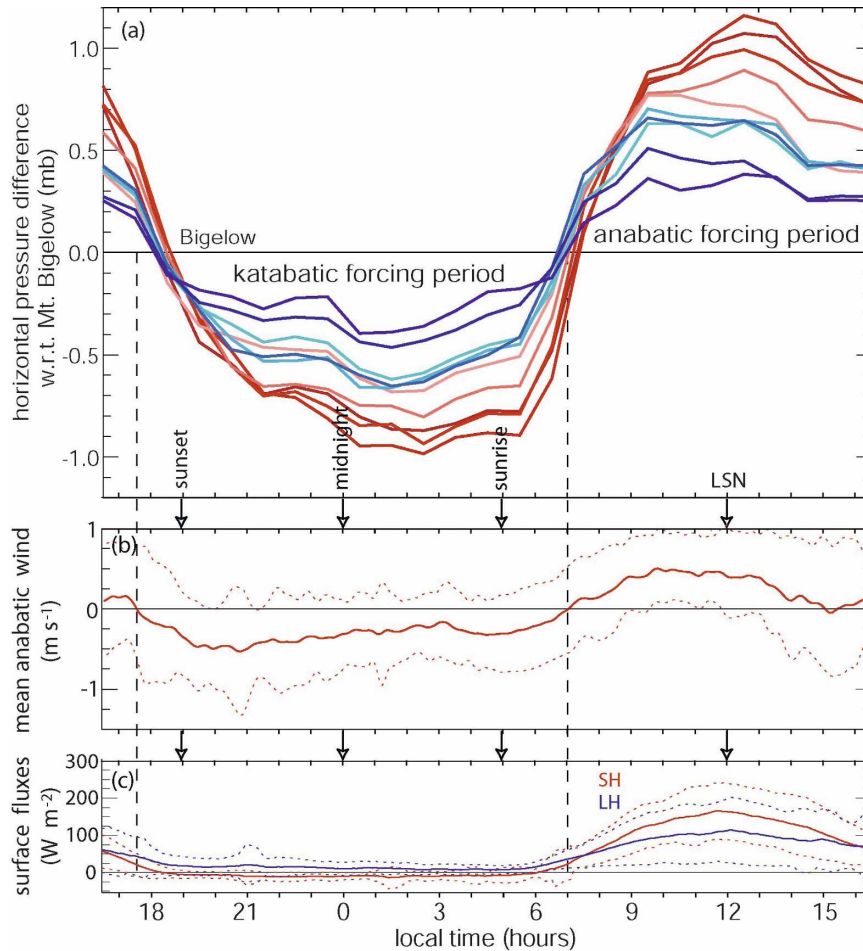


FIG. 5. Analysis of diurnal variation for the 58-day period. (a) Horizontal pressure difference between Mt. Bigelow and the 10 surrounding ISFF stations. The line colors match station label colors in Fig. 2. (b) The mean anabatic wind based on the 10 ISFF stations. (c) The surface sensible and latent heat (LH) fluxes, based on four ISFF flux stations. In (b) and (c), the solid lines are the averages, the dashed lines are the averages ± 1 std dev. The dashed vertical lines across (a)–(c) mark the start and end times of the mean anabatic wind period.

anomalously warm in the second half of the night and anomalously cool in the afternoon. The temperature variation at the Mt. Lemmon astronomical observatory is not as reliable, the probe apparently was exposed to the sun, thus the daytime heating is exaggerated (Fig. 4c), and therefore also the negative T' at night. Station 2 has the largest diurnal temperature range, because of its low elevation, and because it is located in a local valley (Fig. 2): cold air drains, thus this station records the strongest cool anomaly near sunrise. Local terrain concavity matters (Geerts 2003): a station such as station 9 on a slight local ridge on the piedmont east of the Santa Catalina Mountains is relatively warm near sunrise (Fig. 4d).

As discussed in section 2b, the observed differences in p'' (Fig. 4b) cannot be interpreted as horizontal pres-

sure differences. The hydrostatic horizontal pressure difference $(\partial p/\partial r)\Delta r$ between Mt. Bigelow and the surrounding stations is estimated using (5), and its diurnal variation is shown in Fig. 5a. A clear diurnal cycle is present, with about the same magnitude as that for differences in p'' , but the phase has shifted: the lowest pressure occurs over the mountain (relative to the surrounding stations) close to LSN, about 5 h later than the maximum p'' deficit over the mountain (Fig. 4b). The period when the horizontal pressure difference is negative (lower pressure at Mt. Bigelow) is referred to as the anabatic forcing period. This period starts 2 h after sunrise, peaks close to LSN, and ends shortly before sunset (Fig. 5a). Its counterpart, the “katabatic forcing period,” peaks between midnight and sunrise; the katabatic forcing period has a flatter peak than its

anabatic counterpart and lasts some 3 h longer than the nighttime.

The surface heat fluxes in Fig. 5c are an average for the four ISFF stations with flux capability, and for the 58-day period. None of these four stations is located on the mountain. Time series of fluxes derived from the Mt. Bigelow flux tower contained some unrealistically high values even for 30-min averages and thus were not included. It is assumed that the average surface flux from the four foothill stations is representative of the overall mountain area encompassed by the decagon in Fig. 2.

We now examine three details of the diurnal variation of horizontal pressure differences (Fig. 5a). First, the anabatic forcing period seems nearly coincident with the positive surface sensible heat (SH) flux cycle (Fig. 5c), and thus the cycle of net incoming solar radiation at the surface. This seems rather early; in fact its peak occurs a few hours *before* LSN for stations on the east side of the mountain. Thus, the anabatic forcing period for a mountain the width of the Santa Catalina Mountains appears to peak earlier than the sea-breeze forcing, which is proportional to the temperature difference between the marine BL and the CBL over the adjacent landmass, and that difference peaks a few hours *after* LSN (Abbs and Physick 1992). This observation will be revisited.

Second, the slight depression in the composite anabatic forcing period at ~ 1500 local time (LT; 2200–2300 UTC) may be related to thunderstorm activity. Lightning data from the NLDN suggest a strong diurnal modulation of monsoonal thunderstorms in the Tucson, Arizona, area: they almost all occur between 2200 and 0300 UTC (Watson et al. 1994). Orographic thunderstorms may generate a cold pool and pressure rise over the mountain. We revisit this later as well.

And third, we question the validity of one of the findings of Fujita et al. (1962). They studied summertime pressure variations around the San Francisco Peaks, a mountain of similar size near Flagstaff, Arizona. The abstract of Fujita et al. (1962) states that “. . . a very small low-pressure area formed over the heated side of the mountain slope . . .” They attribute the lower pressure on the southeastern slopes in the morning to the higher net radiation and thus a higher surface heat flux at that time. Our data do not confirm this pressure response. The stations on the east side of the Santa Catalina Mountains tend to have the highest pressure relative to Mt. Bigelow 2–3 h before LSN (mostly blue stations in Fig. 5a), while those on the western flanks of the mountain (mostly colored red in Fig. 5a) experience the strongest anabatic wind forcing just after LSN. In

other words, the six eastside stations have a rather high pressure in the morning [-0.2 mb compared to the four westside stations, at 1000 LT, and a lower pressure just after LSN (-0.4 mb at 1300 LT)]. Further evidence comes from the contrast between two stations: 5 (east) and 4 (northwest). They are located at roughly the same elevation on opposite foothills of the Santa Catalina Mountains. In the morning the horizontal pressure difference is negligible (Fig. 6a), while in the evening the eastern station (i.e., 5) actually has a slightly lower pressure, even though, as expected, its temperature perturbation is lower than at the NW station (i.e., 4) at that time (Fig. 6b). The key factor appears to be the small altitude difference between stations 4 and 5 (Fig. 2). Since the prevailing winds were southeasterly during the 58-day period, and the stratification is strongest around dawn (Fig. 7), it is possible that the anomalously high pressure at station 5 (and the other eastside stations) around dawn, compared to that at station 4, is due to some upstream blocking and flow splitting. In short, the horizontal pressure variations are controlled not by slope orientation but mainly by station altitude.

b. Solenoidal forcing

Three different data sources are used to examine the solenoidal forcing [the rhs (6)] over the Santa Catalina Mountains. First, we explore the diurnal variation of θ_v based on station data (Fig. 7). Only 11 stations are shown in Fig. 7; Mt. Lemmon was excluded since its record lacked humidity measurements and its temperature data are of poor quality (section 3a). The diurnal θ_v variation is plotted against altitude; when the CBL is well developed, the x axis in Fig. 7 can be considered to be distance from a (bell shaped) mountain; the lower stations are farther to the right. The nocturnal development of a low-level cold pool is obvious. Little nocturnal cooling occurs at Mt. Bigelow, which was in the residual mixed layer on most days. Of particular interest is the increase of θ_v toward the mountain (toward the left in Fig. 7a) between about 1200–1700 LT, when the CBL is well developed. This provides clear evidence of solenoidal forcing. The mean θ_v difference between Bigelow and the 10 foothill stations during the afternoon (1200–1700 LT) is 1.5 K. Clearly the daytime CBL did not reach above the elevation of Mt. Bigelow on some days in the 58-day period examined here, according to the 0000 UTC TUS soundings (Fig. 3a), thus the excess θ_v at Bigelow could be attributable to vertical stratification. The θ_v anomaly (i.e., the departure from the 11-station mean) for just those days with a deep CBL is shown in Fig. 7b. Mt. Bigelow still is warmer in the afternoon: the mean θ_v difference between Bigelow

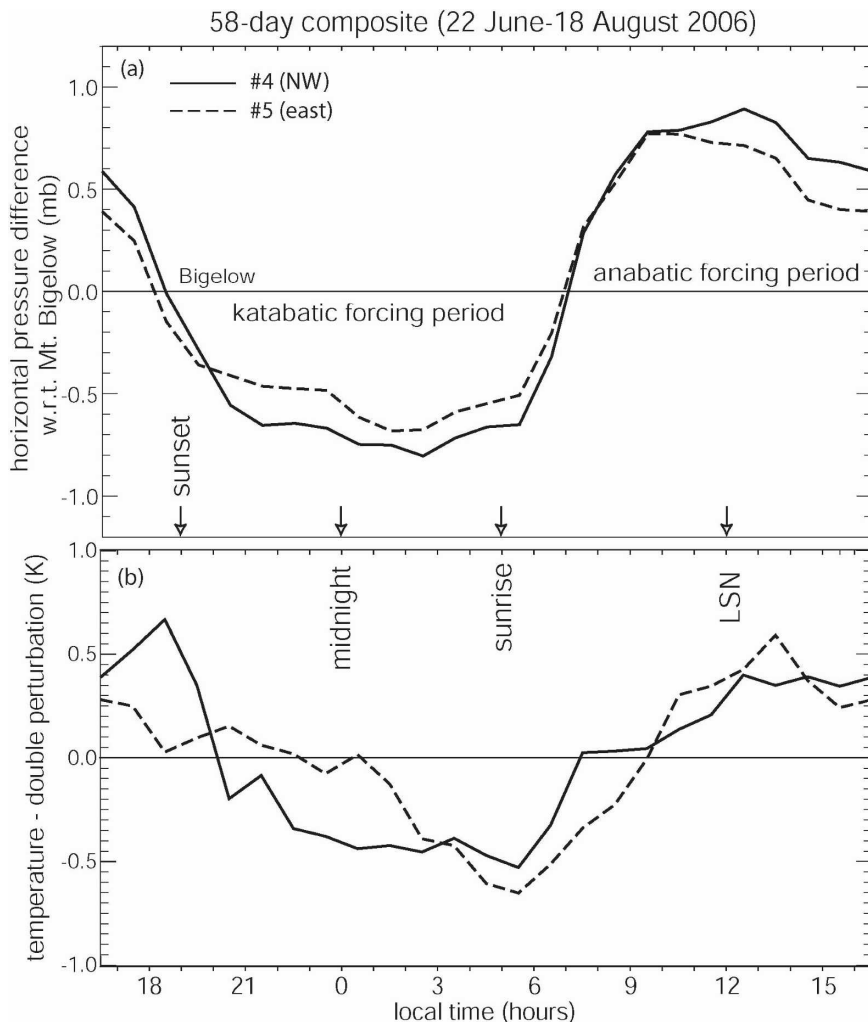


FIG. 6. Diurnal cycle of (a) horizontal pressure difference relative to Mt. Bigelow and (b) double temperature perturbation, for two stations at nearly the same elevation, but on opposite sides of the mountain.

and the 10 foothill stations between 1200 and 1700 LT is 1.2 K for the deep CBL days.

A second piece of evidence for the solenoidal forcing comes from an analysis of the T_v difference between the Mt. Bigelow tower and the corresponding (linearly interpolated) pressure level in the 0000 UTC TUS sounding. The TUS radiosondes are launched from a site located 27 km to the SSE of Mt. Bigelow. The National Weather Service soundings typically are released 55 min before the nominal time, and the ascent rate is 3–4 m s^{-1} , thus we used the 2315 UTC data from Mt. Bigelow in this comparison. At 2315 UTC (3 h and 45 min after LSN) the CBL normally is well developed, and orographic cumulus convection is likely. A total of 55 days of the 58-day period had sounding data at the level of Mt. Bigelow, and for those days T_v was on average

1.40 ± 1.53 K warmer at Mt. Bigelow than at the radiosondes. In comparison, the air was 0.68 ± 1.03 K cooler over Mt. Bigelow than aboard the radiosonde at 1115 UTC (~1 h before sunrise) for 56 of the 58 days with 1200 UTC sounding data. The afternoon sounding–Mt. Bigelow T_v difference corresponds well with the station data θ_v difference mentioned above.

A third piece of evidence for the solenoidal forcing comes from the one day in the CuPIDO campaign that a series of MGAUS radiosonde pairs was released simultaneously from an upwind corner of the Santa Catalina Mountains and from its peak. On this day, 17 August 2006, the mean wind below 5 km MSL was just 1.9 m s^{-1} from 168° , thus the Windy Point release site was generally upwind of Mt. Lemmon (Fig. 2). The soundings were released hourly from 4 h before LSN

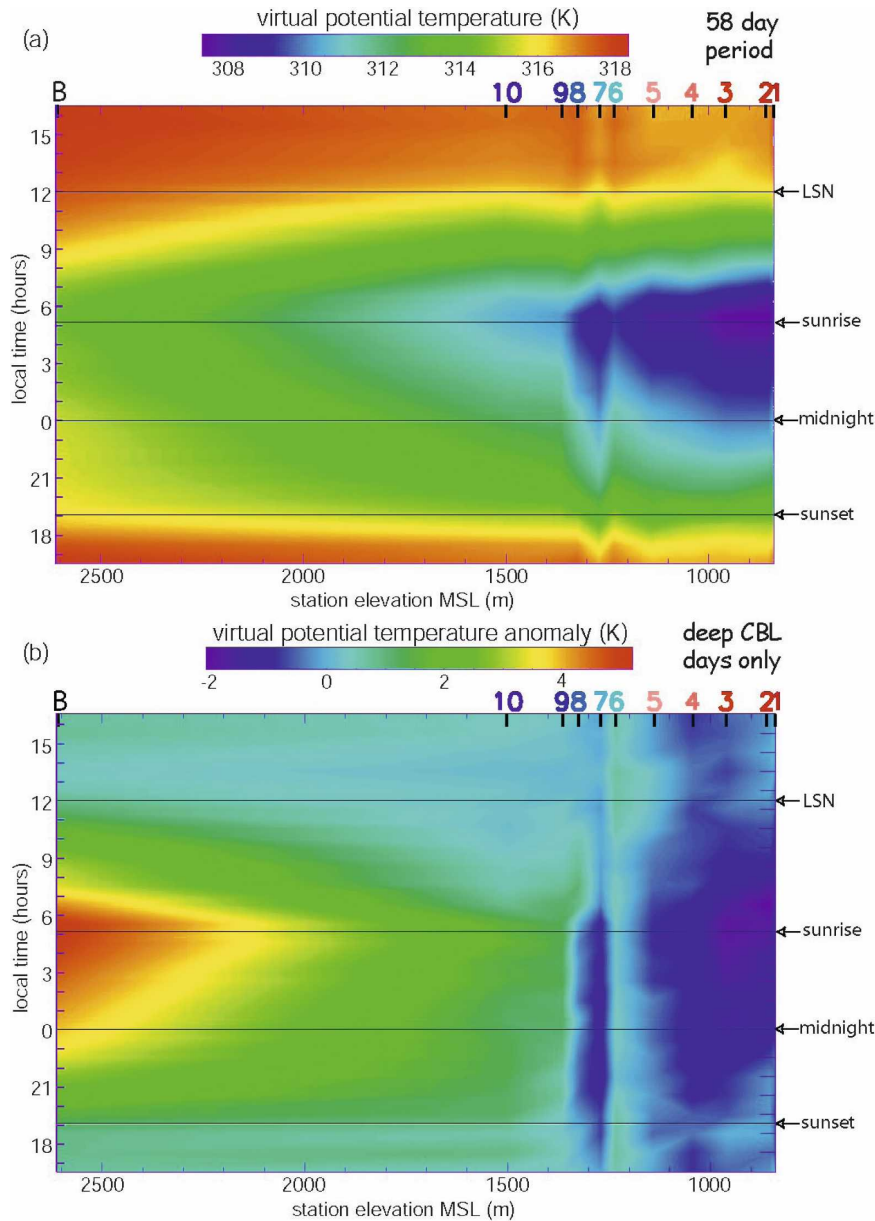


FIG. 7. (a) Diurnal variation of θ_v as a function of station elevation. The tick marks on top indicate the station elevation. (b) As in (a), but showing the θ_v anomaly from the 11-station mean at any one time, and for just those days on which the CBL depth is at least 3 km MSL, according to the 0000 UTC TUS sounding (Fig. 3a).

until LSN (Fig. 8). The average CBL top was *below* the elevation of Mt. Lemmon for the Windy Point soundings, but a shallow CBL did develop above Mt. Lemmon, suggesting a doming CBL top as sketched in Fig. 1. The air was unusually moist for Tucson on this day, with a cumulus cloud base just ~ 250 m above Mt. Lemmon. All Mt. Lemmon soundings ascended through cumuli (explaining the large θ_v variability between soundings), while none of the Windy point soundings pen-

etrated cumuli. Below the cloud base, the Windy Point θ_v was lower than that at Mt. Lemmon in some sounding pairs, and higher in other sounding pairs (Fig. 8a). On average, the low-level θ_v difference was of the expected sign, but insubstantial (< 0.4 K, Fig. 8b). Above the Cu cloud base, larger θ_v excesses over Mt. Lemmon were present at some levels in the composite soundings, reflecting net cumulus buoyancy. The lack of low-level θ_v difference even in the last sounding pair (when the

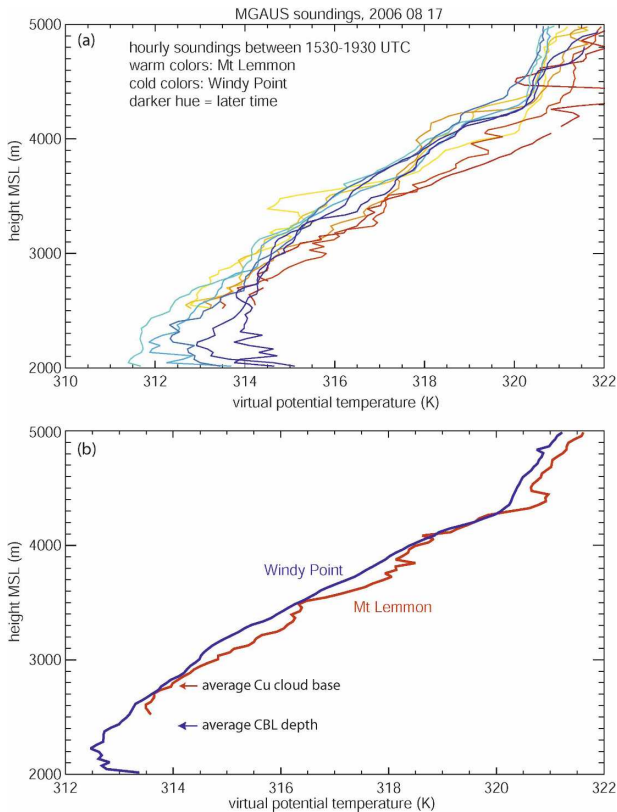


FIG. 8. (a) Profiles of θ_v above Mt. Lemmon and Windy Point based on hourly MGAUS radiosondes released between 1530 and 1930 UTC (LSN is at 1929 UTC) 17 Aug 2006. Windy Point (shown as an “x” in Fig. 2) is on Santa Catalina’s southeastern ridge, at a distance of 10.6 km from Mt. Lemmon. (b) The average of the five soundings shown in (a), for both release sites.

CBL top reaches above Mt. Lemmon) suggest that Windy Point is essentially within the mountain warm core.

These three pieces of evidence confirm the presence of solenoidal forcing with a magnitude of 1–2 K over the width of the mountain. This corresponds with a pressure deficit of 0.5–1.0 mb over the mountain, according to (1). This magnitude chimes with the observed peak horizontal pressure deficit over Mt. Bigelow (Fig. 5a). The pressure difference of 0.5–1.0 mb over a distance of ~ 15 km (the characteristic width of the Santa Catalina Mountains) is comparable to that of solenoidal circulations of matching scales over flat terrain. Florida sea breezes, for instance, are marked by a surface pressure gradient of $0.2\text{--}0.5$ mb $(10\text{ km})^{-1}$ (Atkins and Wakimoto 1997; Kingsmill and Crook 2003). For gust fronts this figure ranges between $1\text{--}2$ mb $(10\text{ km})^{-1}$ (Mueller and Carbone 1987; Atkins and Wakimoto 1997; Kingsmill and Crook 2003).

c. Anabatic wind

Daytime upslope winds over a heated mountain are highly variable, due to turbulence driven by thermals in the CBL. Also, even the slightest mean advective wind in the mountain environment will yield wind toward the mountain on the upwind side of the mountain and vice versa on the opposite side. Thus upslope flow estimation requires data from around the mountain and some temporal averaging. The 10 ISFF stations were generally well positioned around the mountain (Fig. 2) to compute the mean anabatic wind \bar{v}_n and mountain-scale convergence, as defined in Eqs. (7) and (8).

The diurnal variation of the mean anabatic wind in the foothills of the Santa Catalina Mountains is shown in Fig. 5b. The average surface (10 m AGL) flow is katabatic (negative) all night long, starting 1.5 h before sunset and ending 2 h after sunrise, averaging 0.3 m s^{-1} during this period. Anabatic flow picks up swiftly during the morning, peaks 2 h before LSN, and remains rather steady until ~ 1300 LT. At its peak the mean anabatic wind is 0.5 m s^{-1} , which corresponds with a mountain-scale convergence of $0.9\text{ }10^{-4}\text{ s}^{-1}$.

It is interesting to note that most mass convergence occurs *before* LSN, while solar radiation and surface heat fluxes peak at LSN (Fig. 5c) and the surface and BL temperatures typically peak a few hours *after* LSN. In fact the maximum θ_v difference between Mt. Bigelow and the foothills stations occurs at 1430 LT (Figs. 4c and 7). Thus, one would expect that the solenoidal forcing (essentially the horizontal temperature differences in the CBL) for a toroidal heat island circulation around the mountain and the resulting surface anabatic flow and mountain-scale convergence also peak a few hours after LSN. The early development of anabatic wind (Fig. 5b) is roughly consistent with its pressure forcing (Fig. 5a). Apparently mass convergence in the boundary layer over an isolated mountain is not entirely driven by local surface heating.

The anomalously early peaking of the anabatic wind (and its pressure forcing) may be related to cumulus development over the mountain. One can argue that orographic cumulus development causes net deep-column heating and thus low-level hydrostatic pressure decrease and enhanced convergence. Yet three CuPIDO case studies presented in Demko et al. (2009) do not reveal this. By comparing orographic cumulus growth rate with mountain-scale convergence, they show that the only measurable impact of cumulus evolution on mountain-scale near-surface convergence is the divergence following the collapse of a cumulus tower. The 58-day composite seems to confirm this. Near 1500 LT the mean flow briefly becomes slightly

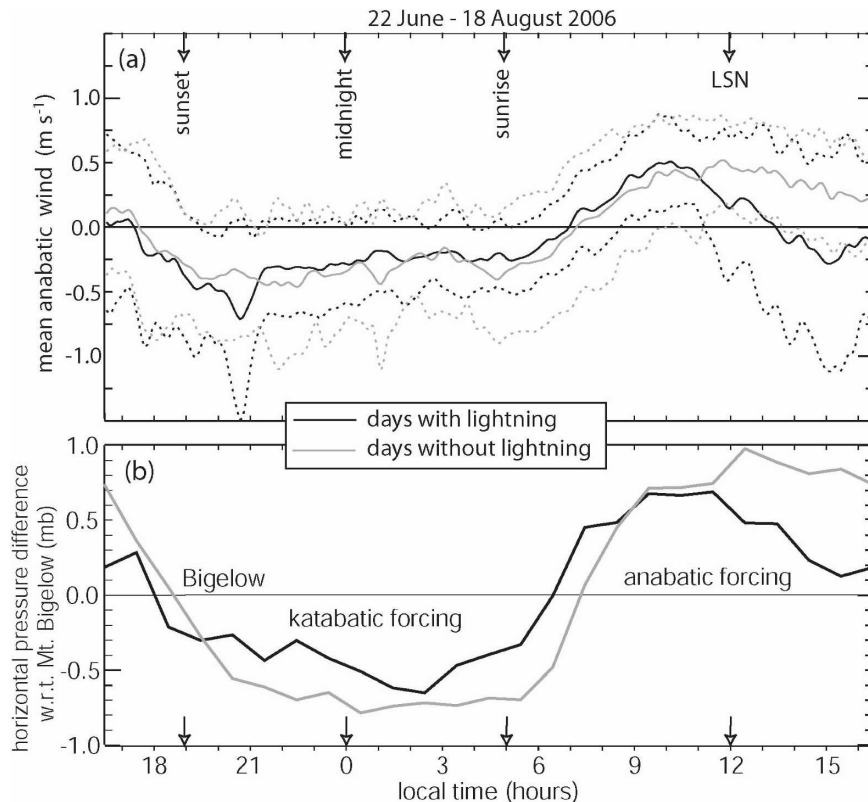


FIG. 9. (a) As in Fig. 5b, but separating between days with lightning and days without lightning recorded by the NLDN within 13 km of Mt. Lemmon between 1200 and 0000 UTC. (b) As in Fig. 5a, but using the same lightning-based separation and grouping data from all 10 ISFF stations into a single average.

katabatic (Fig. 5b). A separation of the 58-day period between days with/without afternoon thunderstorms proves that this divergent flow is a feature of thunderstorm days only (Fig. 9a); the divergence probably is due to the spreading of cold pools from thunderstorms, which usually form in the early afternoon (Fig. 10). It is consistent with the weakened anabatic forcing at this time (Fig. 5a), in particular on thunderstorm days (Fig. 9b), but the effect of thunderstorms is more apparent in the wind field than the pressure difference field, because the cold pool may spread over the foothill stations as well, thus removing the pressure *difference* effect.

d. Impact of the surface sensible heat flux on solenoidal forcing and anabatic wind

Surface heat fluxes were dramatically different between the 2006 premonsoon dry period and the monsoon wet period. This allows us to study their impact on the solenoidal forcing and the resulting circulation (Fig. 11). The peak daytime sensible heat flux halved from ~ 200 to $\sim 100 \text{ W m}^{-2}$ following the heavy rains early in

the wet period (Figs. 11e,j). The latent heat flux increased, but while this may affect moist convection, it does not directly affect the solenoidal forcing. The amplitude of the diurnal surface temperature cycle decreased by about 40% in the wet period (Figs. 11b,g), because of increased cloudiness and soil moisture. The amplitude of p'' differences between stations decreased accordingly, except for Mt. Bigelow (Figs. 11a,f). This comparison yields strong evidence that the observed diurnal pressure variations are driven by surface heating.

The amplitude of the diurnal cycle of the horizontal pressure difference between the foothill stations and Mt. Bigelow also decreased by about 40% from the dry period to the wet period (Figs. 11c,h), and its phase remained essentially unchanged. The nocturnal katabatic wind was substantially stronger during the dry period (Figs. 11d,i), which is consistent with the higher nocturnal cooling rate. Nocturnal cloudiness and rainfall were not uncommon during the wet period.

The daytime mean anabatic wind was *not* substantially stronger during the premonsoon dry period. The

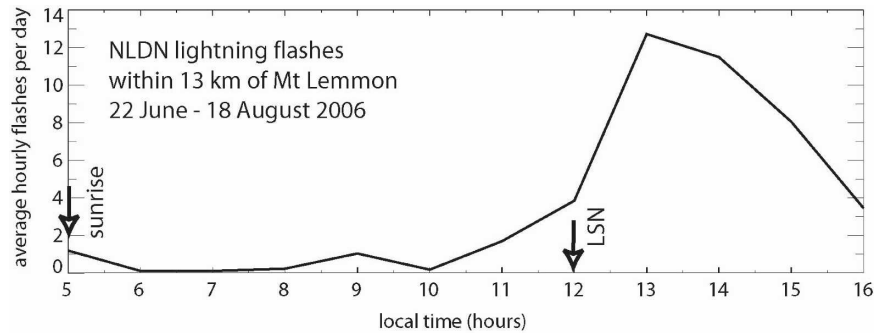


FIG. 10. Diurnal variation of lightning over the Santa Catalina Mountains, according to NLDN data.

transition from katabatic to anabatic wind was steeper during the dry period, consistent with the rapid transition from katabatic to anabatic pressure forcing (Fig. 11c) and the rapid increase in surface sensible heat flux (Fig. 11e). Also, the anabatic wind was more likely to continue into the afternoon during the dry period, compared with the monsoon period (Figs. 11d,i), presumably because fewer thunderstorms erupted. But in both periods, the anabatic wind and its horizontal pressure forcing started about 2 h after sunrise and the anabatic wind peaked 1–2 h before LSN.

In short, this comparison indicates that daytime sensible heat flux strongly controls the amplitude of the solenoidal forcing (expressed in terms of a θ_v difference or horizontal pressure difference), but the strength of the resulting mountain-scale convergence appears less sensitive to surface heating, at least for the Santa Catalina Mountains in summer. We hypothesize that this lack of sensitivity is due to the fact that excessive surface heating increases the chances of moist convection, which produces divergent flow around the mountain. We explore this hypothesis further in the next section.

4. Discussion

One finding of this study is that the mountain-scale convergence peaks 1–2 h *before* LSN over the Santa Catalina Mountains during a 58-day period in summer 2006. Not many publications have examined the diurnal cycle of thermally driven mountain-scale upslope wind. Whiteman (2000) makes a distinction between “mountain–plain” circulations and smaller-scale “slope” wind. A schematic illustration on p. 179 in Whiteman (2000) indicates that *upslope* wind tends to peak as early as 0800 LT, and plain–mountain *upvalley* wind at 1400 LT. The thermally forced circulation around the Santa Catalina Mountains should probably be classified as a mountain–plain circulation, given its size, although

slope winds are likely to occur close to the steep flanks of this mountain range.

There is both theoretical and observational evidence that mountain-scale upslope flow and convergence peak later for larger mountain ranges. The theoretical argument simply is based on a scaling of (6). According to (6), the time τ needed to reach a surface anabatic wind of magnitude V_n scales as

$$\tau = \frac{2V_n\theta_v L}{g\Delta\theta_v H}, \quad (9)$$

where L and H are the length and depth scales of the solenoidal circulation. Thus, for the Santa Catalina Mountains ($L = 15$ km; $H = 2$ km), a solenoidal circulation with an observed strength of $V_n = 0.5$ m s⁻¹ should develop quasi-instantaneously for the observed $\Delta\theta_v$ of 1.5 K ($\tau \sim 2.5$ min). This estimate ignores frictional retardation, but in any event, according to (9), the time scale increases linearly with the mountain width.

The observational evidence is limited. To our knowledge there are no studies of diurnal flow around a mountain with weak winds and a deep CBL. Banta (1984) studied upslope flow development on the lee side of a ~ 25 -km-wide, elongated mountain range in Colorado in midsummer. Upslope (easterly) flow developed shortly after sunrise and peaked before LSN, while downslope (westerly) flow prevailed in the afternoon. Banta (1984) explained this wind reversal by the mixing of westerly momentum from aloft as the CBL deepened. He speculated that convergence peaked over the mountain range before LSN, and moved eastward later on. Over the Big Island of Hawaii, which is 140 km in diameter, the mountain-scale surface convergence started 2–3 h after sunrise and peaked at 1200–1400 LT during 45 summer days in 1990 (Chen and Nash 1994). But this case differed from the present

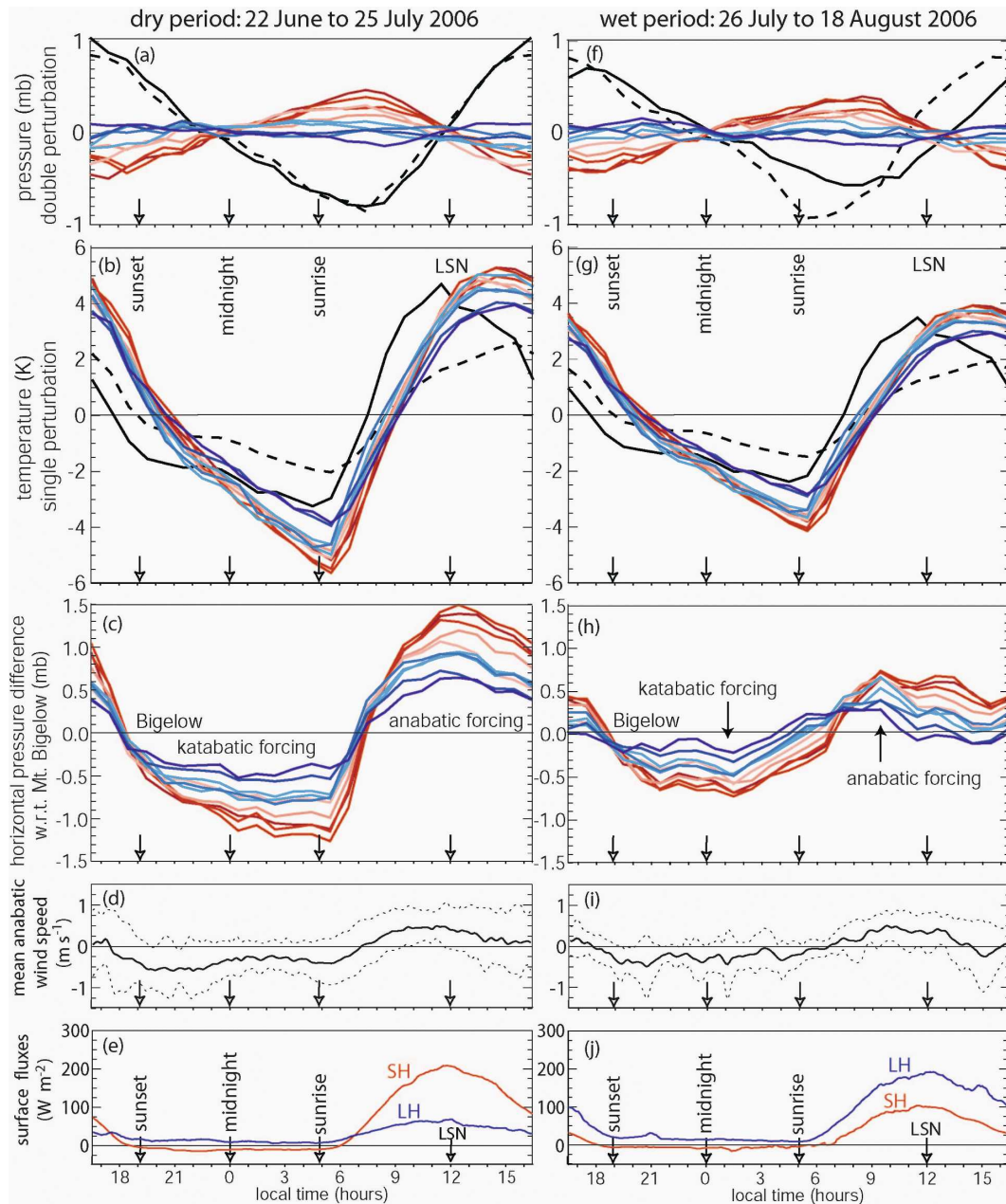


FIG. 11. Comparison of diurnal patterns for the (left) premonsoon dry period and (right) the monsoon wet period. (a), (f) The pressure perturbation p'' , (b), (g) the temperature departure from the 24-h mean, and (c), (h) the horizontal pressure difference with Mt. Bigelow for all stations, color coded as in Fig. 2. The solid (dashed) lines in the top four panels represent Mt. Lemmon (Mt. Bigelow). Shown in the bottom four panels are the mean anabatic wind (d), (i) ± 1 std dev and (e), (j) the average surface heat fluxes.

study over the Santa Catalina Mountains in that the flow was generally blocked (the Froude number was small, generally below 0.2), and the depth of the toroidal flow was limited to the trade wind inversion, which was always below the mountain top. Observations and simulations over the eastern Andes indicate that the

anabatic flow from the Amazon toward the Bolivian Altiplano peaks a few hours after LSN and terminates after sunset (Egger et al. 2005; Zängl and Egger 2005). The scale of this circulation exceeds 100 km. Numerical simulations of plateau–plain circulations suggest that the solenoidal circulation is delayed and the plateau

heat low is more persistent for wider and less elevated plateaus (Zängl and Chico 2006).

For a mountain the size of the Santa Catalina Mountains (30-km diameter), our findings suggest that mountain-scale convergence, and possibly the (hydrostatic) horizontal pressure gradient that forces the anabatic flow, peak just before LSN. In section 3c we suggested that the early development of anabatic flow apparent in the *composite* is the result of orographic cumulus development: on days with thunderstorms the mountain-scale convergence becomes negative (divergent) in the afternoon, due to outflow spreading. Yet on days without thunderstorms the anabatic flow peaks close to LSN and stays positive all afternoon (Fig. 9a).

It may appear counterintuitive that orographic thunderstorms somehow suppress the heat low over the mountain (Fig. 9b) and the anabatic flow (Fig. 9a). One can argue that towering cumuli or a cumulonimbus (Cb) detrain “rich” BL air (high in θ_e) into the midtroposphere, between the level of free convection and the level of neutral buoyancy, and that this should lead to net column heating and hydrostatic pressure reduction over the mountain. This argument implies that moist convection at least temporarily enhances low-level convergence. We do find that convergence and the upslope horizontal pressure gradient are slightly stronger in the morning on thunderstorm days compared to days without thunderstorms (Fig. 9), but they become weaker at a rather early time (after 1100 LT), as the earliest thunderstorms erupt (Fig. 10).

These findings are consistent with three other publications. The surface pressure observations by Fujita et al. (1962) indicate that the mountain low dissipates by the time of the first Cb formation, even before a cold pool forms. An analysis of aircraft data by Raymond and Wilkening (1982) also indicates that mediocre and even deep orographic cumulus convection does not enhance the strength of the low-level convergence. And, as mentioned above, Demko et al. (2008) find no enhanced convergence during the cumulus growth stages, but divergence occurs during the decay of deep cumuli.

We cannot conclude that the enhanced convergence leads to orographic convection, but we can conclude that orographic convection suppresses the mass (and thus moisture and energy) influx needed to sustain itself. Self-suppression characterizes thunderstorms in a weakly sheared environment over flat terrain (e.g., Weisman and Klemp 1982). Decaying “airmass” thunderstorms are associated with surface divergence and a high pressure anomaly. Orographic convergence and convection are geographically fixed, so it is possible that on thunderstorm days the orographic convergence is more sustained under stronger deep-layer mean

wind, so the cold pools drift off. This may yield multiple orographic thunderstorm developments, as is sometimes observed (e.g., Zehnder et al. 2006).

The synergy between pressure perturbations, orographic BL circulations, and cumulus convection over mountains (Fig. 1) remains poorly understood. In a separate paper, we plan to examine the relation between surface heating, mountain-scale convergence, and orographic convection over the Santa Catalina Mountains by means of numerical simulations.

5. Conclusions

Surface and upper-air data collected in summer around the Santa Catalina Mountains (about 30 km in diameter, peaking about 2 km above the surrounding plains) have been used to study the thermal forcing of orographic circulations and associated deep convection. A horizontal pressure gradient is derived from hydrostatic balance for use in the study of diurnal wind forcing in complex terrain. The main findings are as follows:

- The diurnal variation of mountain-scale convergence, with katabatic, divergent surface flow at night and anabatic, convergent flow during the day is in phase with the diurnal variation of the horizontal pressure gradient force, which points toward the mountain during the day and away from the mountain at night.
- The mean anabatic wind near the surface peaks at about 0.5 m s^{-1} , which corresponds with a mountain-scale convergence of nearly $1 \times 10^{-4} \text{ s}^{-1}$ for the Santa Catalina Mountains.
- The daytime pressure deficit over the mountain of 0.5–1.0 mb is hydrostatically consistent with the observed 1–2-K virtual potential temperature excess over the mountain.
- Doubling the daytime surface sensible heat flux increases the diurnal amplitude of temperature and horizontal pressure gradient, but it hardly affects the strength of the mean anabatic wind, at least in an environment where orographic cumulus convection is likely.
- Slightly enhanced convergence and pressure gradient force toward the mountain do occur on mornings before thunderstorms erupt, but this enhancement vanishes by the time thunderstorms develop. The most poignant impact of orographic thunderstorms is mountain-scale divergence, presumably because of the spreading of the storm outflows.

Acknowledgments. This work was funded by National Science Foundation Grant ATM-0444254 and benefited from discussions with Thomas Parish and Joseph Zehnder.

REFERENCES

- Abbs, D., and W. Physick, 1992: Sea-breeze observations and modeling—A review. *Aust. Meteor. Mag.*, **41**, 7–19.
- Atkins, N. T., and R. M. Wakimoto, 1997: Influence of the synoptic-scale flow on sea breezes observed during CaPE. *Mon. Wea. Rev.*, **125**, 2112–2130.
- Bader, D. C., and T. B. Mckee, 1983: Dynamical model simulation of the morning boundary layer development in deep mountain valleys. *J. Appl. Meteor.*, **22**, 341–351.
- Baines, P. G., 1979: Observations of stratified flow past three-dimensional barriers. *J. Geophys. Res.*, **84**, 7834–7838.
- Banta, R. M., 1984: Daytime boundary layer evolution over mountainous terrain. Part I: Observations of the dry circulations. *Mon. Wea. Rev.*, **112**, 340–356.
- , 1986: Daytime boundary layer evolution over mountainous terrain. Part II: Numerical studies of upslope flow duration. *Mon. Wea. Rev.*, **114**, 1112–1130.
- Chen, Y. L., and A. J. Nash, 1994: Diurnal variation of surface airflow and rainfall frequencies on the island of Hawaii. *Mon. Wea. Rev.*, **122**, 34–56.
- Damiani, R., and Coauthors, 2008: The Cumulus, Photogrammetric, In Situ, and Doppler Observations Experiment of 2006. *Bull. Amer. Meteor. Soc.*, **89**, 57–73.
- Demko, J. C., B. Geerts, Q. Miao, and J. Zehnder, 2008: Boundary layer energy transport and cumulus development over a heated mountain: An observational study. *Mon. Wea. Rev.*, in press.
- de Wekker, S. F. J., S. Zhong, J. D. Fast, and C. D. Whiteman, 1998: A numerical study of the thermally driven plain-to-basin wind over idealized basin topographies. *J. Appl. Meteor.*, **37**, 606–622.
- Egger, J., and Coauthors, 2005: Diurnal circulation of the Bolivian Altiplano. Part I: Observations. *Mon. Wea. Rev.*, **133**, 911–924.
- Fujita, T., K. A. Styber, and R. A. Brown, 1962: On the meso-meteorological field studies near Flagstaff, Arizona. *J. Appl. Meteor.*, **1**, 26–42.
- Geerts, B., 2003: Empirical estimation of the monthly-mean daily temperature range. *Theor. Appl. Climatol.*, **74**, 145–165.
- Grubišić, V., and B. J. Billings, 2007: The intense lee-wave rotor event of Sierra Rotors IOP 8. *J. Atmos. Sci.*, **64**, 4178–4201.
- Hagan, M. E., J. M. Forbes, and A. D. Richmond, 2002: Atmospheric tides. *The Encyclopedia of Atmospheric Sciences*, J. R. Holton, J. Pyle, and J. A. Curry, Eds., Academic Press, 159–165.
- Holton, J. R., 2004: *An Introduction to Dynamic Meteorology*. 4th ed. Academic Press, 535 pp.
- Houze, R. A., 1993: *Cloud Dynamics*. Academic Press, 573 pp.
- Hunt, J. C. R., and W. H. Snyder, 1980: Experiments on stably and neutrally stratified flow over a model three-dimensional hill. *J. Fluid Mech.*, **96**, 671–704.
- Kingsmill, D. E., and N. A. Crook, 2003: An observational study of atmospheric bore formation from colliding density currents. *Mon. Wea. Rev.*, **131**, 2985–3002.
- Mahrt, L., 1982: Momentum balance of gravity flows. *J. Atmos. Sci.*, **39**, 2701–2711.
- Mass, C. F., and G. K. Ferber, 1990: Surface pressure perturbations produced by an isolated mesoscale topographic barrier. Part I: General characteristics and dynamics. *Mon. Wea. Rev.*, **118**, 2579–2596.
- McNider, R. T., and R. A. Pielke, 1981: Diurnal boundary-layer development over sloping terrain. *J. Atmos. Sci.*, **38**, 2198–2212.
- Miao, Q., and B. Geerts, 2007: Finescale vertical structure and dynamics of some dryline boundaries observed in IHOP. *Mon. Wea. Rev.*, **135**, 4161–4184.
- Mueller, C. K., and R. E. Carbone, 1987: Dynamics of a thunderstorm outflow. *J. Atmos. Sci.*, **44**, 1879–1898.
- Raymond, D., and M. Wilkening, 1980: Mountain-induced convection under fair weather conditions. *J. Atmos. Sci.*, **37**, 2693–2706.
- , and —, 1982: Flow and mixing in New Mexico mountain cumuli. *J. Atmos. Sci.*, **39**, 2211–2228.
- Reiter, E. R., 1982: Typical low-tropospheric pressure distributions over and around the plateau of Tibet. *Arch. Meteor. Geophys. Bioclimatol., Ser. A*, **31**, 323–327.
- , and M. Tang, 1984: Plateau effects on diurnal circulation patterns. *Mon. Wea. Rev.*, **112**, 638–651.
- Smith, R. B., 1980: Linear theory of stratified hydrostatic flow past an isolated mountain. *Tellus*, **32**, 348–364.
- Thyer, N. H., 1966: A theoretical explanation of mountain and valley winds by a numerical method. *Meteor. Atmos. Phys.*, **15**, 318–348.
- Tucker, D. F., 1999: The summer plateau low pressure system of Mexico. *J. Climate*, **12**, 1002–1015.
- Vosper, S. B., 2000: Three-dimensional numerical simulations of strongly stratified flow past conical orography. *J. Atmos. Sci.*, **57**, 3716–3739.
- Watson, A. I., R. E. López, and R. L. Holle, 1994: Diurnal cloud-to-ground lightning patterns in Arizona during the Southwest Monsoon. *Mon. Wea. Rev.*, **122**, 1716–1725.
- Weisman, M., and J. Klemp, 1982: The dependence of numerically simulated convective storms on vertical wind shear and buoyancy. *Mon. Wea. Rev.*, **110**, 504–520.
- Whiteman, C. D., 2000: *Mountain Meteorology: Fundamentals and Applications*. Oxford University Press, 376 pp.
- Zängl, G., and J. Egger, 2005: Diurnal circulation of the Bolivian Altiplano. Part II: Theoretical and model investigations. *Mon. Wea. Rev.*, **133**, 3624–3643.
- , and S. G. Chico, 2006: The thermal circulation of a grand plateau: Sensitivity to the height, width, and shape of the plateau. *Mon. Wea. Rev.*, **134**, 2581–2600.
- Zehnder, J. A., L. Zhang, D. Hansford, A. Radzan, N. Selover, and C. M. Brown, 2006: Using digital cloud photogrammetry to characterize the onset and transition from shallow to deep convection over orography. *Mon. Wea. Rev.*, **134**, 2527–2546.